Avalanches in compressed porous SiO_2-based materials

Guillaume F. Nataf
Departament d'Estructura i Constituents de la Matèria, Facultat de Física, Universitat de Barcelona, Diagonal 647, E-08028 Barcelona, Catalonia, and INP Grenoble, 38031 Grenoble Cedex 1, France

Pedro O. Castillo-Villa, Jordi Baró, Xavier Illa, Eduard Vives, and Antoni Planes
Departament d'Estructura i Constituents de la Matèria, Facultat de Física, Universitat de Barcelona, Diagonal 647, E-08028 Barcelona, Catalonia

Ekhard K. H. Salje
Department of Earth Sciences, University of Cambridge, Downing Street, Cambridge CB2 3EQ, United Kingdom
(Received 23 May 2014; published 15 August 2014; corrected 21 August 2014)

The failure dynamics in SiO_2-based porous materials under compression, namely the synthetic glass Gelsil and three natural sandstones, has been studied for slowly increasing compressive uniaxial stress with rates between 0.2 and 2.8 kPa/s. The measured collapsed dynamics is similar to Vycor, which is another synthetic porous SiO_2 glass similar to Gelsil but with a different porous mesostructure. Compression occurs by jerks of strain release and a major collapse at the failure point. The acoustic emission and shrinking of the samples during jerks are measured and analyzed. The energy of acoustic emission events, its duration, and waiting times between events show that the failure process follows avalanche criticality with power law statistics over ca. 4 decades with a power law exponent $\varepsilon \simeq 1.4$ for the energy distribution. This exponent is consistent with the mean-field value for the collapse of granular media. Besides the absence of length, energy, and time scales, we demonstrate the existence of aftershock correlations during the failure process.

DOI: 10.1103/PhysRevE.90.022405 PACS number(s): 62.20.mm, 61.43.Gt, 89.75.Da, 05.65.+b

I. INTRODUCTION

Crackling noise is encountered in a wide range of systems when a material is subjected to external forces with jerky responses spanning over a wide range of sizes and energies, usually in form of avalanches [1]. Typical examples are magnetization processes [2], martensitic transitions [3,4], plastic deformation in solids [5,6], or materials failure [7,8]. Upon variation of an external field, avalanches of the conjugated properties show a spectacular absence of time and length scales. Crackling noise is often related to critical behavior of avalanches, which stem from intrinsic inhomogeneities or by jamming of microstructures [9]. The failure of porous materials subjected to compressional forces has recently received much attention due to its relevance in the collapse forecast of both natural and artificial structures such as mines, buildings, or bones. It has been shown that when mining materials are subjected to a compressive stress, failure can be heralded by a significant precursor activity [10]. In this precursor regime, the response of the system to the applied compressive stress is not smooth and continuous as classically expected for elastoplastic materials but instead occurs as a sequence of avalanches. Experimentally, it has been shown that the avalanches stem from sudden changes of the internal strain field (displacement discontinuities), which usually lead to shrinking of the sample and can be detected by measuring the acoustic emission (AE) originating from contraction. Avalanche behavior has been observed previously in porous Vycor glass [10], natural goethite [11], porous alumina [12], and berlinite [13]. Their statistical characteristics share many similarities with seismicity such as the Earth crust failure due to stresses originated from plate tectonics [14,15]. These similarities go beyond the avalanche statistics (power law distribution of energies with an exponent near $\varepsilon \simeq 1.4$) and include the statistics of aftershocks and waiting times of acoustic emission or earthquakes [16]. More specifically, it is shown that the Gutenberg-Richter law, the modified Omori' s law, the law of aftershock productivity, and the universal scaling law for the waiting time distribution typically used in statistical seismology hold in Vycor in a broad range of at least six decades of jerk energies with exponents similar to those obtained in earthquakes. Similar results were found in other collapsing minerals.

Theoretical modeling of the nonequilibrium collapse of porous materials is in its infancy with few proposed approaches [17,18]. Models have only considered deformation driven situations with lateral pressure, which is not always the case found in nature or laboratory conditions. It is an aim of our investigations to establish first a firm experimental base on which such models can be founded and by which their results can be tested. It is important to focus here on specific issues such as the porosity of the materials and their topological structures. We consider in this paper simple chemical compounds, all SiO_2 based, to avoid the influence of the chemical variability of the samples. SiO_2-based minerals are abundantly found in the Earth's crust and are used as building materials and substrates for electronic devices. We compare the collapse under compression of synthetic SiO_2 materials, Gelsil, and three natural sandstone rocks under uniaxial compression with slow compression rate. The results are seen in context with those previously obtained in porous Vycor [10,16], which has similar porosity as Gelsil but possesses a different mesostructure.

The paper is organized as follows. In Sec. II we provide basic sample information and briefly describe the experimental

TABLE I. Pore characteristics of the studied materials and Vycor. Data for Gel2.6, Gel5, and Vyc are from Ref. [23]. The density of quartz is 2.648 g/cm^3.

	Gel2.6	Gel5	LGsan	Rsan	Ysan	Vyc
Average pore diameter	2.6 nm	5.0 nm	∼0.05 mm	<0.1 mm	<0.1 mm	7.5 nm
Density (g/cm^3)	∼1.6	∼1.2	∼2.3	∼2.2	∼2.3	∼1.5
Porosity ϕ	0.36	0.54	0.13	0.17	0.17	0.40

setup. The obtained results for the two Gelsil specimens and for sandstone are described in Sec. III. In Sec. IV the obtained results together with results for Vycor are discussed. Finally, in the last section we summarize the main conclusions of the work.

II. EXPERIMENTAL

A. Synthesis and characterization of the samples

We performed uniaxial compression experiments on mesoporous silica ceramics: Gelsil 2.6 (Gel2.6), Gelsil 5 (Gel5), light-gray sandstone (LGsan), red sandstone (Rsan), and yellow sandstone (Ysan) with rates ranging from 0.2 to 2.8 kPa/s.

Gelsil monoliths are produced (4F International Co., Gainesville, FL) in a sol-gel process by hydrolization of silica containing precursor liquids, followed by condensation and heat treatment. Silica molecules condensate to spheres on stochastic sites within the hydrolized silica precursor. Subsequent gelation, drying, and consolidation leads to a network-like arrangement of pure silica spheres. The voids between these spheres constitute a random network of interconnected corridors and pockets and show a large pore size distribution. Mean void diameters of 2.6 and 5.0 nm are found in Gelsil 2.6 and Gelsil 5, respectively, from N_2-adsorption experiments and BET/BJH analysis[19,20]. Cylinder-shaped samples were cut from the initial Gelsil samples. Before the compression experiments, Gelsil samples were cleaned with a 30% solution of H_2O_2, during 24 h and dried at 130°C.

Prismatic samples were cut from large sandstone hand specimens. The light-gray sandstone used in this study was a Darley Dale sandstone (Derbyshire, England). It is a brown-yellow, well-indurated, feldspathic sandstone with a connected porosity of $(13.3 \pm 0.8)\%$. The modal composition is 69% quartz, 26% feldspar, 3% clay, and 2% mica. The grain size varies from 0.01 to 1 mm and show no discernible preferred orientation. The cementing materials are mainly silicious. The brittle-to-creep transition of these materials was investigated in Ref. [21].

The red sandstone is from Arran (UK) from the Devonian period and is largely the result of the intrusion and uplift of the tertiary granites [22]. It belongs to the lithostratigraphic unit of *old red sandstone* and is of considerable importance to early paleontology for its fossil content. The red color of these rocks arises from the presence of iron oxide. The main components are 79% quartz, 5% feldspar, 11% clay; the cement consists mainly of carbonates. The average grain size is 0.3 mm and the Youngs modulus is ca. 3.2.

The yellow sandstone is from Hopeman Bay near Inverness in Scotland. It is Permian (299–251 my). It is similar in composition to the red sandstone but slightly coarser and less compacted. The main characteristics of the studied specimens here are summarized in Tables I and II. It is interesting to note that the average pore diameter is several orders of magnitude larger in natural sandstones than in synthetic Gelsil and Vycor glasses.

B. Compression and acoustic emission setups

Details of the experimental arrangement for the uniaxial compression tests have been described elsewhere [10]. Samples are placed between two aluminum plates where the bottom plate is hanging from the load cell at the top of the arrangement and is static. The upper plate is pulled downward at constant stress rate $d\sigma/dt$ by guiding rods that slide along three Teflon-covered holes in the bottom plate. Samples have been cut in order to have desired transversal sections, yielding small and similar compression rates (see Table II). Nevertheless, the limitations of the experimental setup requires us to select smaller sections for samples with larger failure strength in order to reach the collapse. Thus, compression rates vary within one order of magnitude. In any case, with these small rates we do not expect to see any dependence, as previously tested for Vycor [10].

A laser extensometer (*Fiedler Optoelektronik*) measures the vertical separation between the plates, h, with a nominal resolution of 100 nm. The load cell (1 kN range) signal is measured with a lock-in amplifier and has been calibrated with standard weights. The resolution is about 1 N. During compressive stress, the release of localized strain energy in the sample through AE is measured. The AE signal is detected by piezoelectrics transducers embedded in the compression plates, centered at a distance of 4 mm from the sample surface. The sensors are encapsulated in stainless steel to reduce electrical noise. They are acoustically coupled with the aluminum plates by a thin layer of vaseline. The

TABLE II. Area, A, and height, H, of the studied samples and failure stress, σ_f, stress rate, $d\sigma/dt$, and number of recorded AE signals, N, in the corresponding experiments.

	A (mm^2)	H (mm)	σ_f (MPa)	$d\sigma/dt$ (kPa/s)	N
Gel2.6(1)	46.7	6.2	1.0	0.7	5412
Gel2.6(2)	16	4.1	0.5	0.8	926
Gel5(1)	35.4	5.3	7.1	2.8	4098
Gel5(2)	31.1	5.8	9.6	1.9	45210
LGsan	29.6	5.9	13.4	2.9	21238
Rsan	17.0	4.3	11.0	2.4	27271
Ysan(1)	37.2	7.2	3.6	1.4	11058
Ysan(2)	70.6	6.3	3.4	0.2	49893
Vyc	13.2	5	30	0.2	10695

signals from the transducers are preamplified (60 dB), band filtered (between 100 kHz and 2 MHz), and transferred to a PCI-2 acquisition system from Europhysical Acoustics (*Mistras group*) working at a time resolution of 40 MHz. The output signal is a voltage $U(t)$. For the identification of signals a threshold above the instrumental noise is set. In our experiments it is fixed at 27 dB. A hit is defined to start with the first crossing of this threshold. The end time of a hit is the time at which the signal voltage falls and remains to below the threshold for more than a preset hit detection time (HDT $= 100\ \mu$s). After the hit is finished the system rearms again in a short time called "hit lockout time" (HLT) fixed to HLT$= 2\ \mu$s, and is ready for the detection of new signals. Changes of these parameters affect very little the analysis presented below. Recently, a detailed analysis of the influence of the threshold, HLT, and HDT parameters on the critical exponents have been presented for the case of AE associated to dislocation movement [24]

The system allows us to determine the energies of the acoustic emission events, which are obtained by fast numerical integration of the square voltage of signals, as

$$E = 1/R \int_{t_i}^{t_f} U^2(t)\, dt, \tag{1}$$

where t_i and t_f are starting and ending times of the signal and $R = 10\,\text{k}\Omega$ is a reference resistance. The duration of the events is given by $T = t_f - t_i$. Waiting times between signals correspond to the elapsed time between starting times of consecutive signals. The AE activity is defined as the number of hits per unit time (measured over intervals of 1 s). The experiment ends a few minutes after the failure stress σ_f has been reached.

III. RESULTS

A. Gelsil

Figure 1 shows as an example time evolution of (a) the sample height, (b) the square of its derivative, (c) the AE activity, (d) the amplitude of AE signals (maximum voltage), (e) their duration, and (f) their energy in Gel2.6(1). Similar results were obtained for Gel2.6(2), Gel5(1), and Gel5(2). AE activity is recorded from the beginning of the experiment. Large amplitude signals with long duration are already detected well before the big crash. The activity decreases considerably just after the big crash. It is worth noting that this effect is less significant in Gelsil 5 samples. The good correlation between the AE activity and the square of the drop velocity, $(dh/dt)^2$, is in agreement with the common recognition that the AE signal is proportional to the dissipated energy during the failure process. Amplitude, duration, and energy vary over several decades during the experiments.

Figure 2(a) shows the energy distributions $p(E)$ in log-log plots for Gelsil 2.6(1). The histogram corresponds to the accumulation of signals along the whole experiment. A good linear behavior is observed over more than four decades, which suggests that the distribution of energies follows a power law in a very good approximation. Thus, the distribution is described

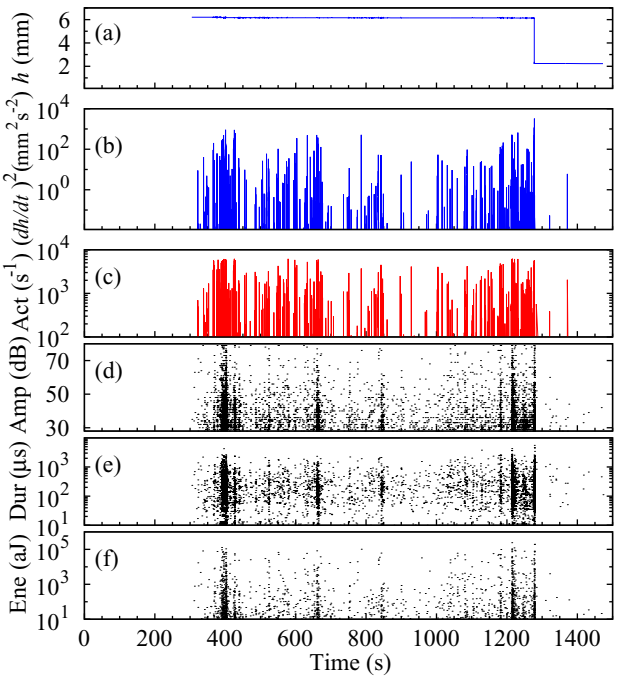

FIG. 1. (Color online) Sample height (a), the square of its time derivative (b), AE activity (c), amplitude (d), duration (e), and energy (f) of AE signals recorded during the compression experiment of the sample of Gel2.6(1). The vertical scales are logarithmic in (b), (c), (e), and (f).

by

$$p(E)dE \simeq \frac{E^{-\epsilon}}{E_{\min}^{1-\epsilon}} dE \quad E > E_{\min}, \tag{2}$$

where $E_{\min}$ is a lower cutoff needed for normalization (and experimentally unavoidable). In order to examine the distribution in more detail we apply the method presented in Ref. [25]. The technique consists of studying the behavior of the power-law exponent, ε, fitted using the maximum likelihood method, as a function of a varying lower cutoff $E_{\min}$. As shown in Fig. 2(b), this analysis leads to a plateau which defines an exponent: $\varepsilon = 1.37 \pm 0.03$.

The distribution of aftershocks (AS) for selected energy intervals for Gelsil 2.6(1) are shown in so-called Omori plots in Fig. 3(a). We have considered as main shocks (MS) all events with energies E_{MS} within predefined intervals from 10^k to 10^{k+1} aJ, with $k = 0$, 1, 2, and 3. After each MS we study the sequence of subsequent events until an event with an energy larger than the energy of the MS is found, which terminates the sequence of AS. We divide the time line from the MS toward the future in intervals, for which we count the number of AS in each of them. Figure 3(b) shows the same data given in Fig. 3(a) after rescaling the vertical axis. The data collapse into a single curve when the AS activity is normalized as $r_{\text{AS}} {E_{\text{MS}}}^{2\alpha/3}$. The optimum scaling gives the values of the productivity exponent α and the Omori exponent p characterizing the slope. The exponent α is usually related to ε through $\varepsilon = 1 + 2\alpha/3$ [26]. We obtain $\alpha = 0.5 \pm 0.1$, consistent with the energy exponent, $\varepsilon = 1.37$. The best fit for the Omori exponent is $p = 0.71 \pm 0.04$.

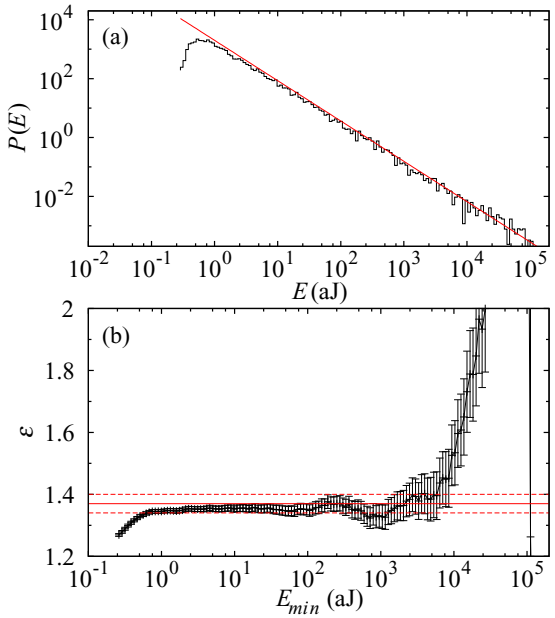

FIG. 2. (Color online) (a) Log-log plot of the energy distribution of the AE events and (b) fitted energy exponent as a function of the lower fitting cut-off recorded for the sample of Gel2.6(1). The solid lines in (a) and (b) define the value of the fitted energy exponent, $\varepsilon = 1.37 \pm 0.03$, and the dashed lines in (b) represent the error limits.

Figure 4 shows the distribution of waiting times, defined as $\delta_j = t_j - t_{j-1}$, with j labeling only the events with energy larger than a given threshold energy $E_{\min}$. The axes are scaled as $\langle r(E_{\min})\rangle\delta$ and $D(\delta, E_{\min})/\langle r(E_{\min})\rangle$, where $\langle r(E_{\min})\rangle$ is the mean number of events per unit time with an energy $E \geqslant E_{\min}$. This leads to a collapse of data in a single curve showing double power-law behavior with exponents $1 - \nu$ for small arguments, and $2 + \xi$ for large arguments. In the present case we have

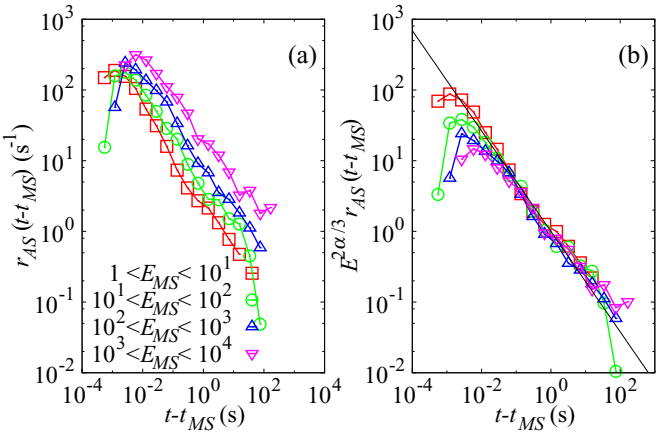

FIG. 3. (Color online) (a) Number of aftershocks per unit time as a function of the time distance to the main shock for the sample of Gel2.6(1). Different symbols indicate different MS energy windows in aJ. The number of sequences averaged is 2343 for $1 < E_{\rm MS} < 10^1$ (squares), 1077 for $10^1 < E_{\rm MS} < 10^2$ (circles), 487 for $10^2 < E_{\rm MS} < 10^3$ (triangles up), and 195 for $10^3 < E_{\rm MS} < 10^4$ (triangles down). (b) Scaled plot with productivity exponent $\alpha = 0.5$. The thin solid line defines the slope $p \simeq 0.71$.

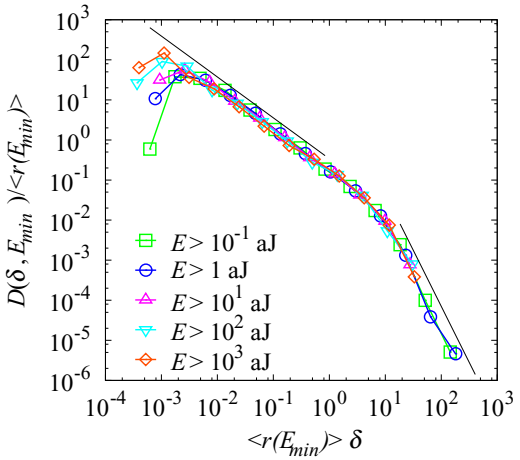

FIG. 4. (Color online) Distribution of waiting times for different values of $E_{\min}$ from the experiments with the sample of Gel2.6(1). The thin solid lines correspond to the exponents $1 - \nu \simeq 1.02$ (left) and $2 + \xi \simeq 2.8$ (right). The number of signals studied is 5412 for $E > 10^{-1}$ aJ (squares), 4225 for $E > 1$ aJ (circles), 1882 for $E > 10^1$ aJ (triangles up), 805 for $E > 10^2$ aJ (triangles down), and 318 for $E > 10^3$ aJ (diamonds).

found $(1 - \nu) = 1.02 \pm 0.05$ and $(2 + \xi) = 2.8 \pm 0.3$. This scaling leads to a double power-law master curve as proposed in Ref. [27] for systems with nonstationary activity rate. The lack of stationary character is evident in Fig. 1(c).

Gel5(1) and Gel5(2) samples show very similar results to Gel2.6(1). The corresponding exponents are shown in Table III. In Gel2.6(2) we find data that are consistent with the values in Table III although with very large error bars. Therefore, this sample has not been considered for the discussion of the power law exponents.

B. Sandstones

Compared with Gelsil, the acoustic activity in sandstone is smaller in the early stages of the experiments and gradually increases near the big crash. The time evolution of (a) the sample height, (b) the square of its derivative, (c) the AE activity, (d) the amplitude of AE signals (maximum voltage), (e) their duration, and (f) their energy corresponding to LGsan is shown in Fig. 5. In Rsan, relatively large shrinking events have been detected already before the big crash. These events give rise to a localized increase of acoustic activity similar to the increase observed in the vicinity of the big crash. This is shown in the second example reported in Fig. 6. In any case, the distribution of event energies is similar in all sandstone samples as compared with Gelsil. Data corresponding to LGsan depicted in Fig. 7(a) on a log-log scale. The figure shows good power-law behavior over almost five decades. Figure 7(b) shows the fitted exponent as a function of the cut-off energy. Compared to Gelsil results, a flat plateau is not well defined for sandstones. In this case an effective exponent should be determined from the vertical position of the shoulder revealed by this curve. A value $\varepsilon = 1.48 \pm 0.08$ was estimated which is, within errors, compatible with the energy exponents obtained in Gelsil.

TABLE III. Exponents fitted individually for the different samples studied in this work, as explained in the text. Data for Vycor from Ref. [16] is also shown for comparison.

	ϵ	p	α	$1-\nu$	$2+\xi$
Gel2.6(1)	1.37 ± 0.03	0.71 ± 0.04	0.5 ± 0.1	1.02 ± 0.05	2.8 ± 0.3
Gel5(1)	1.35 ± 0.03	0.70 ± 0.04	0.5 ± 0.1	1.01 ± 0.05	—
Gel5(2)	1.37 ± 0.03	0.77 ± 0.02	0.60 ± 0.05	1.09 ± 0.05	3.02 ± 0.08
LGsan	1.48 ± 0.08	0.78 ± 0.04	0.8 ± 0.1	0.86 ± 0.05	2.0 ± 0.1
Rsan	1.55 ± 0.05	0.74 ± 0.04	0.8 ± 0.1	1.12 ± 0.02	2.3 ± 0.1
Ysan(1)	1.44 ± 0.05	—	0.7 ± 0.1	1.04 ± 0.05	1.4 ± 0.2
Ysan(2)	1.49 ± 0.05	0.74 ± 0.08	0.7 ± 0.1	1.01 ± 0.05	1.8 ± 0.2
Common scaling	1.4	0.75	0.6	1.0	2.5
Vycor [16]	1.40 ± 0.05	0.75 ± 0.1	0.5 ± 0.1	0.93 ± 0.05	2.45 ± 0.08

The distribution of aftershocks for different energy intervals for LGsan is shown in Fig. 8(a). While the power-law behavior is not as extended as for Gelsil, an exponent $p = 0.78 \pm 0.04$ is measured with a large error bar. The optimum scaling is obtained with productivity exponent $\alpha \simeq 0.8 \pm 0.1$, which is different from the exponent obtained for Gelsil. Nevertheless, the measured α and ε exponents satisfy, within the errors the scaling relation, $\varepsilon = 1 + 2\alpha/3$. Figure 8(b) shows the distribution of waiting times for selected values of the threshold energy. We fitted exponents $1 - \nu = 0.86 \pm 0.05$ and $2 + \xi = 2.0 \pm 0.1$, which are shown by continuous lines in Fig. 8(b). Similar data were obtained for the rest of sandstone samples and are presented in Table III.

In this section we presented data for experiments chosen as representative examples, describing the behavior of Gelsil and sandstone samples. All results are fully reproducible for specimens cut from the same initial sample with similar geometry. Even more so, no statistical differences arise when, for each material, data corresponding to all specimens were analyzed together. This is an important result that indicates that scale invariance of the avalanches during compression is independent of the compression rate, at least within the range of rates of our experiments.

IV. COMPARISON WITH VYCOR AND DISCUSSION

We now compare the results obtained in Gelsil and sandstones with previously reported results for porous Vycor 7930 (Corning Inc., NY) in Refs. [10] and [16]. Results for Vycor stem from an experiment [16] performed at a

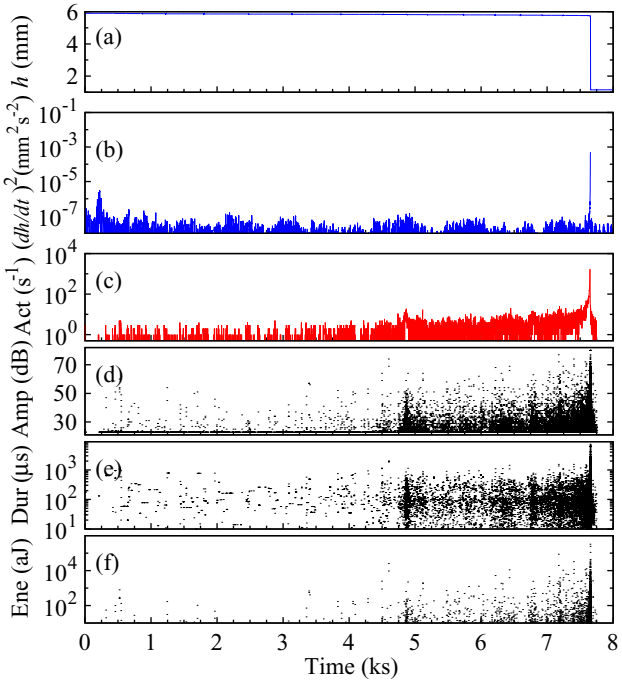

FIG. 5. (Color online) Sample height (a), the square of its derivative (b), AE activity (c), amplitude (d), duration (e), and energy (f) of AE signals recorded during the compression experiment of the sample of LGsan. The vertical scales are logarithmic in (b), (c), (e), and (f).

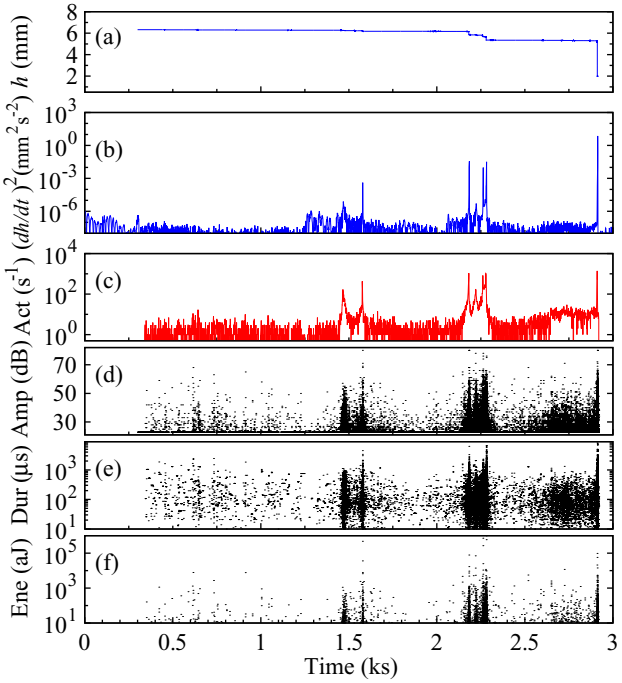

FIG. 6. (Color online) Sample height (a), the square of its derivative (b), AE activity (c), amplitude (d), duration (e), and energy (f) of AE signals recorded during the compression experiment of the sample of Rsan. The vertical scales are logarithmic in (b), (c), (e), and (f).

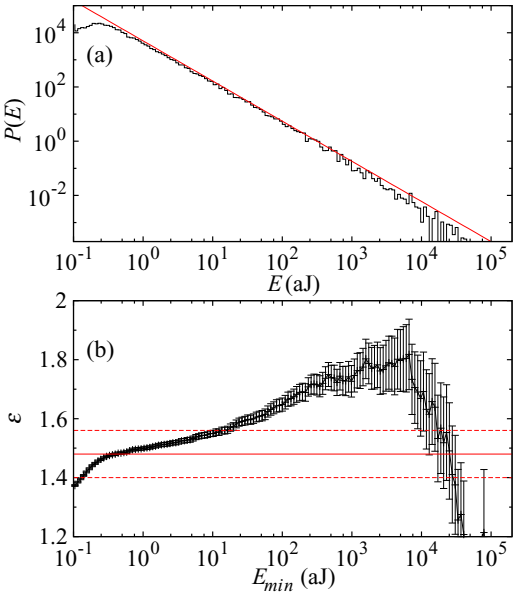

FIG. 7. (Color online) (a) Log-log plot of the energy distribution of the AE events and (b) energy exponent $\varepsilon \simeq 1.48 \pm 0.08$ as a function of the lower fitting cut-off recorded for the sample of LGsan. The solid line defines the value of the effective critical exponent and the dashed lines represent the error.

compression rate of 1.6 kPa/s. Specific features of the Vycor sample are given in Tables I and II. Vycor is, like Gelsil, a porous SiO_2-ceramic but synthesized using a different method that yields a different meso-porous structure. Vycor 7930 is synthesized via a temperature-induced phase separation

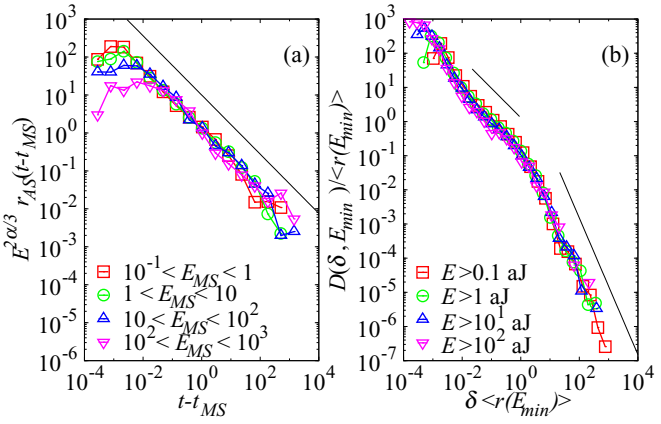

FIG. 8. (Color online) (a) Scaled representation of number of aftershocks per unit time as a function of the time distance to the main shock for the sample LGsan. Best collapse corresponds to $\alpha = 0.84$. The continuous line indicates the fitted slope $p \simeq 0.78$. The symbols indicate the different MS energy windows in aJ. The number of sequences averaged are 426 for $10^{-1} < E_{\rm MS} < 1$ (squares), 755 for $1 < E_{\rm MS} < 10^1$ (circles), 136 for $10^1 < E_{\rm MS} < 10^2$ (triangles up), and 46 for $10^2 < E_{\rm MS} < 10^3$ (triangles down). (b) Scaled representation of the waiting times distribution. The continuous lines define the exponent $1 - \nu = 0.86$ (left) and $2 + \xi = 2.0$ (right). The number of data analyzed is 1401 for $E > 0.1$ aJ (squares), 975 for $E > 1$ aJ (circles), 220 for $E > 10$ aJ (triangles up), and 80 for $E > 100$ aJ (triangles down).

of Na_2O-B_2O_3-SiO_2 melt. After cooling, the Ba_2O_3-rich phase is leached out with an acidic solution, which leaves a 96% pure SiO_2 skeleton [28] containing cylindrical pores randomly distributed in length, density, and angle. The mean ratio of pore diameter d over pore length l was found to be $d/l \geqslant 0.23$ [29]. Pores of our sample show an average diameter of 7.5 nm and a rather narrow pore-size distribution. While Gelsil and sandstone are granular porous materials, Vycor has a nongranular structure constituted of a continuous glass skeleton. The fact that compressive failure strength is expected to depend to a large extent on the adherence between grains [30] could explain why the failure strength (for similar porosities) is much higher in Vycor than in Gelsil or Sandstone (see Table II).

In spite of different failure strengths (see Table II), all statistical properties of compressive avalanches in Vycor, Gelsil, and the studied sandstones are very similar. In Fig. 9(a) we compare the corresponding energy distributions. The plot showing the energy exponent as a function of the lower energy cut-off [Fig. 9(b)] reveals some interesting differences, however. The plateau is very well defined over more than five decades for Vycor. Gelsil shows a similar quality of the power-law fit, while results in sandstone are clearly less defined. The effective power-law exponent is defined at the value of the initial shoulders in Fig. 9(b), around $\varepsilon \simeq 1.45$. The fact that we observe an interval with a small slope instead of a clear plateau in sandstone could be a consequence of the complex mixing relationship of the different components of the natural sandstones. In fact, both Gelsil and sandstones can be classified as granular materials, while Vycor that

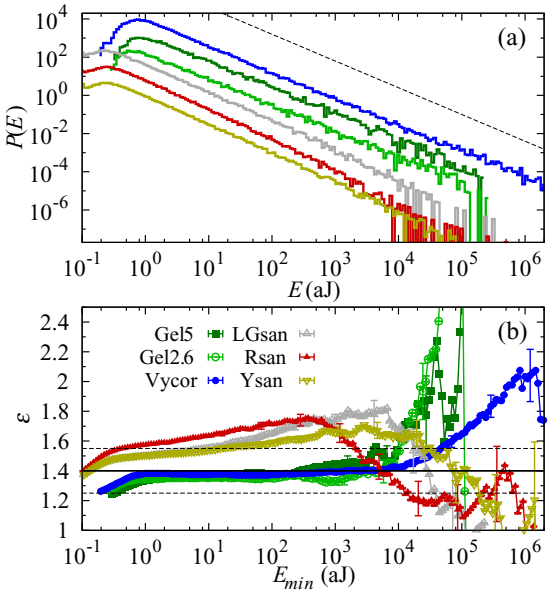

FIG. 9. (Color online) (a) Log-log plot of the energy distribution of the AE events. From top to bottom curves correspond to the following samples, respectively: Vycor, Gel5, Gel2.6, LGsan, Rsan, and Ysan. For the sake of clarity, except for Vycor, the curves are shifted. (b) Corresponding fitted energy exponents as a function of the lower fitting cut-off recorded for the same samples. The symbols correspond to Vycor (empty circles), Gel5 (squares), Gel2.6 (solid circles), LGsan (empty up triangle), Rsan (solid up triangle), and Ysan (down triangle). Only few representative error bars are shown.

has an interconnected structure does not qualify as *granular* in geometrical terms. In granular materials failure under uniaxial compression occurs by means of a double mechanism: breaking of bonds and relative grain displacements, which involves friction. Only bond breaking occurs in Vycor. We suggest that when only bond breaking occurs the system displays criticality; that is, the failure process occurs under the absence of characteristic scales. The relative importance of the two mechanisms in granular materials determines the deviations from criticality. In Gelsil, the friction mechanism is less important due to a strong adherence between SiO_2 grains. As a consequence, this material displays critical behavior to a very good approximation. In contrast, sandstones are sedimentary rocks constituted of grains composed mainly of quartz (SiO_2), which are cemented together by other minerals. In this case, the adherence of the grains is much less strong and friction occurs during the failure process that result in deviations from criticality.

Nevertheless, despite the differences described above, a power-law behavior over almost three decades with $\varepsilon \simeq 1.4 \pm 0.1$ is still rather well defined in all samples. This exponent ε has been estimated within mean field theory [31]. The values $\varepsilon_c^{\mathrm{MF}} = 1.33$ and $\varepsilon_{\mathrm{cum}}^{\mathrm{MF}} = 1.66$ are obtained depending on whether the distribution of avalanche energies corresponds to a small region close to the critical point or to a cumulated distribution over the whole variation of the driving field. In our case, in spite that ε is measured from the cumulated distribution, our value is closest to $\varepsilon_c^{\mathrm{MF}}$. In contrast to a standard MF theory approach, a critical value of the pressure is difficult to define in a compression experiment. One might be tempted to consider the failure stress as the critical point, but the AE activity displays almost-diverging peaks (associated to small collapses) well before the big crash in a series of multifragmentation processes, which overlap with each other. This is specially clear in Vycor [10,16], Gelsil [see Fig. 1(b)], and Rsan [see Fig. 6(b)], where the evolution does not show a unique increasing trend toward the big failure. This suggests that SiO_2-based porous materials may be permanently near a critical point, or kinetically crossing many times through it, during compression. This can be visualized if the system self-organizes itself into a dynamical critical point irrespective of the applied force. This point of view is consistent with previous studies which suggest that the exponent ε does not change when data subsets corresponding to different time windows of experimental data are analyzed. [16].

It is interesting to compare the distribution of avalanche durations for the different materials. The expected power-law behavior is less obvious, although still visible in Fig. 10(a). A plateau is not observed in the likelihood plots for any of our materials. The determination of AE avalanche durations is experimentally very challenging indeed. The real strain avalanches can be much distorted by the emission, propagation, and detection of signals with the sensor. In particular, the limited sensor response introduces exponential convolutions to the physical avalanche shape. In addition, the threshold used in the AE measurements affect the measured durations, which is then more related to the amplitude of the avalanches than to their *true* duration.

Despite this problem, the distribution $P(D)$ in Fig. 10(a) can be seen to include an effective power-law regime over 1–2 decades with an exponent $\tau \simeq 2$. This exponent also agrees with the mean-field value reported in Ref. [31].

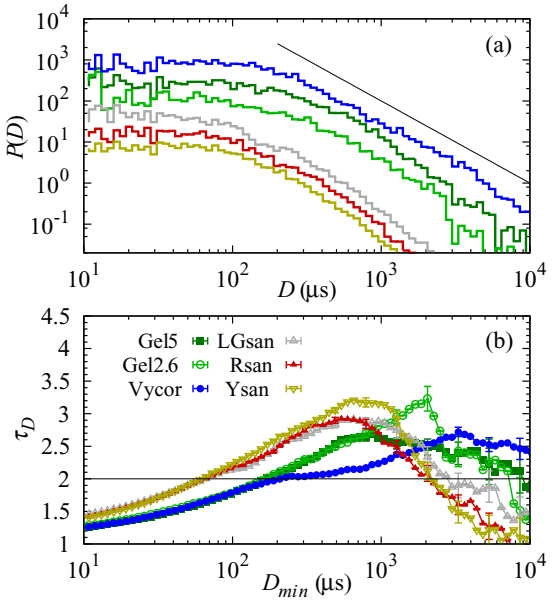

FIG. 10. (Color online) (a) Log-log plot of the distribution of durations of AE events. From top to bottom data corresponds to the following samples, respectively: Vycor, Gel5, Gel2.6, LGsan, Rsan, and Ysan. Curves have been shifted vertically for clarity, except for Vycor. The continuous straight line correspond to the expected mean-field behavior. (b) Corresponding fitted duration exponents, τ, as a function of the lower fitting cut-off recorded for the same samples. Symbols correspond to the different samples according to the legend in Fig. 9.

Omori's plots are shown in Fig. 11 in a scaled representation for all materials investigated in this study and Vycor. Note that here the vertical and horizontal axes are scaled by $\langle r \rangle$, that is the total number of signals recorded during each experiment divided by the total duration. A common scaling can be obtained with a productivity exponent $\alpha = 0.63$, which corresponds, approximately, to the average value of the productivity exponents obtained for Gelsil and Vycor ($\alpha \simeq 0.5$) and sandstones ($\alpha \simeq 0.7$). This averaged exponent is indeed consistent with the averaged energy exponent, $\epsilon \simeq 1.4$.

The scaled waiting time distributions for Gelsil, sandstone, and Vycor are shown in Fig. 12. The six curves collapse to a very good approximation into the same master double power-law curve with exponents $1 - \nu \simeq 1$ and $2 + \xi \simeq 2.5$. This double power-law behavior is reproducible for all samples. The observed variation of the exponent $2 + \xi$ obtained independently for each sample is due to the sensitivity of this exponent to a limited range of values of the activity rate.

It has recently been shown [16] that there is a strong relationship between the statistics of AE during the compression of porous Vycor and the statistics of earthquakes. The AE signals and the earthquake waiting time distributions follow a single scaled curve with exponents $1 - \nu$ and $2 + \xi$ to be the same in Vycor and earthquakes. The activity rate is not stationary in compression experiments (it can span almost four orders of magnitude) from the beginning of the experiments to the big crash, collapsing of AE and earthquake data was possible using data from earthquake catalogues of regions with quite

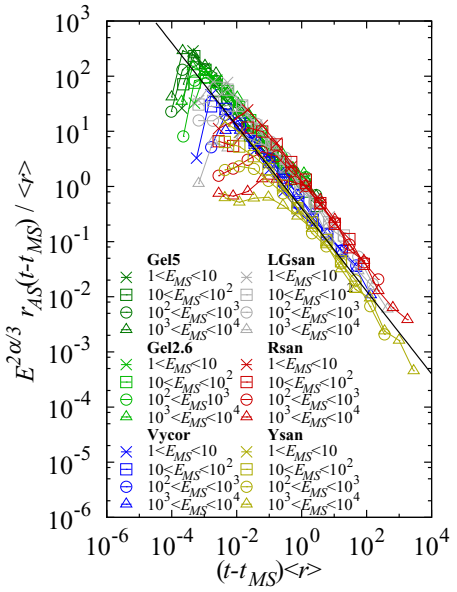

FIG. 11. (Color online) (a) Scaled representation of the number of aftershocks per unit time as a function of the time distance to the mainshock (Omori's plot) for all the studied Gelsil and sandstone samples. Results for Vycor are also included. The best scaling has been found with a productivity exponent $\alpha = 0.6$. The slope of the thin continuous line is $p = 0.75$. Energy values in the legend are expressed in aJ.

broad distribution of activity rates. Present results enable us to extend such a conclusion to the case of Gelsil and sandstones, which are hence within the same universality class.

An AE study of rock fracture has been recently reported by Davidsen [14]. In that work, several porous natural

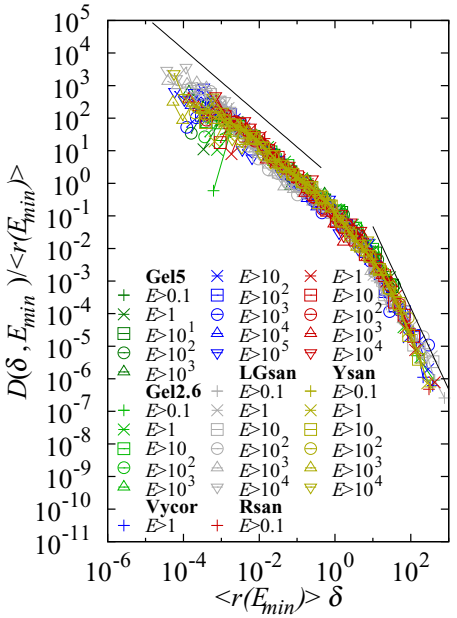

FIG. 12. (Color online) Scaled plot of the distribution of waiting times for different values of $E_{\min}$ from Gelsil, sandstones, and Vycor samples. The continuous lines define the (average) exponents $1-\nu \simeq 1$ and $2+\xi \simeq 2.5$. Energy values in the legend are expressed in aJ.

materials were studied, including Flechtingen sandstone with 7% porosity, Bleuerswiller sandstone with 24% porosity, among others. Experiments were performed at constant strain rate (instead of constant stress rate, as in our case) and the statistical analysis was restricted to periods of stationary activity. The data were scaled with the expected γ function [$P(\theta) \sim \theta^{1-\gamma}\exp(-\theta/B)$, where θ is the scaling variable]. The scaling function was shown to be indistinguishable from that of earthquakes. Moreover, the value reported for the exponent $1-\gamma$ is much smaller than our exponent $1-\nu$, which might indicate the existence of weaker time correlations between waiting times in these stationary periods of activity. We have analyzed periods of stationary activity in Gelsil 2.6 and Vycor and we have found that in this case the distribution of waiting times also scales, to a reasonably good approximation, to a γ function with the same parameters θ and B obtained in Ref. [14].

V. SUMMARY AND CONCLUSIONS

We have studied fracture dynamics of synthetic and natural porous materials subjected to uniaxial compression. All the studied materials are SiO_2-based with different characteristics of the porosity structure. AE has been used to monitor the fracture process together with the simultaneous measurement of the sample height. AE signals are well correlated with rapid (discontinuous) changes of the sample height, which correspond to local avalanches. AE signals start to be detected far before the big crash associated with the catastrophic fracture, which takes place at a given fracture strength.

Similar critical behavior is obtained for all SiO_2 studied materials. It has been possible to determine a set of critical exponents common to the different samples that determine energy distributions, aftershock time correlations, and waiting times distributions. The fact that the exponents associated with the energy and duration distributions (ε and τ) are close to the expected mean-field exponents suggests that avalanche criticality in compressed SiO_2-based porous materials display mean-field behavior (to a good approximation), despite the fact that the position of the critical point is difficult to identify from the data. Nevertheless, the corroboration of this hypothesis certainly requires more detailed investigations. The behavior in SiO_2-porous materials is different from other porous materials such as goethite [11], berlinite [13], or alumina [12], which are also granular materials.

The observation that all SiO_2-based porous materials appear to display the same dynamical features suggests that the dominant underlying physics of the avalanche formation in the same SiO_2-based system, but possibly not in goethite, berlinite, and alumina. This scenario is also consistent with the robustness of the universality of the shape of the scaling function of the waiting times of SiO_2-based materials.

ACKNOWLEDGMENTS

We thank Wilfried Schranz for supplying and characterizing the Gelsil samples. We acknowledge financial support from the Spanish Ministry of Science (Grant No. MAT2013-40590-P). E.K.H.S. is grateful to EPSRC (Grant No. RG66344) and the Leverhulme Foundation (Grant No. RG66640) for support.

[1] J. P. Sethna, K. A. Dahmen, and C. R. Myers, Nature **410**, 242 (2001).
[2] G. Durin and S. Zapperi, in *The Science of Hysteresis*, edited by G. Bertotti and I. Mayergoyz, Vol. II (Academic Press, San Diego 2006), pp. 181–267.
[3] E. Vives, J. Ortín, L. Mañosa, I. Ràfols, R. Pérez-Magrané, and A. Planes, Phys. Rev. Lett. **72**, 1694 (1994).
[4] M. C. Gallardo, J. Manchado, F. J. Romero, J. del Cerro, E. K. H. Salje, A. Planes, E. Vives, R. Romero, and M. Stipcich, Phys. Rev. B **81**, 174102 (2010).
[5] F. F. Csikor, C. Motz, D. Weygand, M. Zaiser, and S. Zapperi, Science **318**, 251 (2007).
[6] J. Weiss, T. Richeton, F. Louchet, F. Chmelik, P. Dobron, D. Entemeyer, M. Lebyodkin, T. Lebedkina, C. Fressengeas, and R. J. McDonald, Phys. Rev. B **76**, 224110 (2007).
[7] S. Zapperi, A. Vespignani, and H. E. Stanley, Nature (London) **388**, 658 (1997).
[8] J. Aué and J. Th.M. de Hosson, J. Mater. Sci. **33**, 5455 (1998).
[9] E. K. H. Salje, X. Ding, Z. Zhao, T. Lookman, and A. Saxena, Phys. Rev. B **83**, 104109 (2011).
[10] E. K. H. Salje, D. E. Soto-Parra, A. Planes, E. Vives, M. Reinecker, and W. Schranz, Philos. Mag. Lett. **91**, 554 (2011).
[11] E. K. H. Salje, G. I. Lampronti, D. E. Soto-Parra, J. Baró, A. Planes, and E. Vives, Am. Min. **98**, 609 (2013).
[12] P. O. Castillo-Villa, J. Baró, A. Planes, E. K. H. Salje, P. Sellappan, W. M. Kriven, and E. Vives, J. Phys. Cond. Matter **25**, 292202 (2013).
[13] G. Nataf, P. O. Castillo-Villa, P. Sellappan, W. M. Kriven, E. Vives, A. Planes, and E. K. H. Salje, J. Phys. Condens. Matter **26**, 275401 (2014).
[14] J. Davidsen, S. Stanchits, and G. Dresen, Phys. Rev. Lett. **98**, 125502 (2007).
[15] H. Kawamura, T. Hatano, N. Kato, S. Biswas, and B. K. Chakrabarti, Rev. Mod. Phys. **84**, 839 (2012).
[16] J. Baró, A. Corral, X. Illa, A. Planes, E. K. H. Salje, W. Schranz, D. E. Soto-Parra, and E. Vives, Phys. Rev. Lett. **110**, 088702 (2013).
[17] L. Girard, J. Weiss, and D. Amitrano, Phys. Rev. Lett. **108**, 225502 (2012).
[18] F. Kun, I. Varga, S. Lennartz-Sassinek, and I. G. Main, Phys. Rev. Lett. **112**, 065501 (2014).
[19] J. Koppensteiner, W. Schranz, and M. R. Puica, Phys. Rev. B **78**, 054203 (2008).
[20] J. Koppensteiner, *The Glass Transition in Nanoscaled Confinement Probed by Dynamic Mechanical Spectroscopy* (Universität Wien, Vienna, 2009).
[21] M. J. Heap, P. Baud, P. G. Meredith, A. F. Bell, and I. G. Main, J. Geophys. Res. **114**, B07203 (2009).
[22] P. F. Friend, W. B. Harland, and J. D. Hudson, Trans. Edinburgh Geol. Soc. **19**, 363 (1963).
[23] J. Koppensteiner, W. Schranz, and M. A. Carpenter, Phys. Rev. B **81**, 024202 (2010).
[24] M. A. Lebyodkin, I. V. Shashkov, T. A. Lebedkina, K. Mathis, P. Dobron, and F. Chmelik, Phys. Rev. E **88**, 042402 (2013).
[25] A. Clauset, C. Shalizi, and M. Newman, SIAM Rev. **51**, 661 (2009).
[26] A. Helmstetter, Phys. Rev. Lett. **91**, 058501 (2003).
[27] A. Corral, Phys. Rev. E **68**, 035102 (2003).
[28] T. H. Elmer, *Engineered Materials Handbook* (ASM International, Ohio, 1992), Vol 4, pp. 427–432.
[29] P. Levitz, J. Chem. Phys. **95**, 6151 (1991).
[30] J.-Y. Delenne, V. Topin, and F. Radjai, Acta Mech. **205**, 9 (2009).
[31] E. K. H. Salje and K. A. Dahmen, Annu. Rev. Condens. Matter Phys. **5**, 233 (2014).